

Breaking network connectivity leads to ultralow thermal conductivities in fully dense amorphous solids

Jeffrey L. Braun, Sean W. King, Ashutosh Giri, John T. Gaskins, Masanori Sato, Takemasa Fujiseki, Hiroyuki Fujiwara, and Patrick E. Hopkins

Citation: *Applied Physics Letters* **109**, 191905 (2016); doi: 10.1063/1.4967309

View online: <http://dx.doi.org/10.1063/1.4967309>

View Table of Contents: <http://scitation.aip.org/content/aip/journal/apl/109/19?ver=pdfcov>

Published by the [AIP Publishing](#)

Articles you may be interested in

[Limits to Fourier theory in high thermal conductivity single crystals](#)

Appl. Phys. Lett. **107**, 203112 (2015); 10.1063/1.4935987

[Simultaneous measurement of thermal conductivity and heat capacity of bulk and thin film materials using frequency-dependent transient thermoreflectance method](#)

Rev. Sci. Instrum. **84**, 034902 (2013); 10.1063/1.4797479

[Size-dependent electroluminescence from Si quantum dots embedded in amorphous SiC matrix](#)

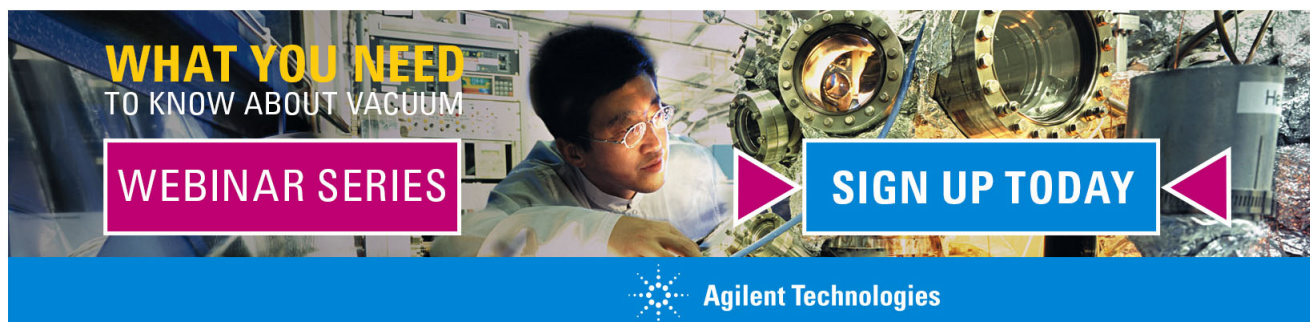
J. Appl. Phys. **110**, 064322 (2011); 10.1063/1.3641989

[Temperature dependent thermal conductivity of Si/SiC amorphous multilayer films](#)

Appl. Phys. Lett. **96**, 093103 (2010); 10.1063/1.3337093

[Amorphous silicon thin-film transistors with field-effect mobilities of \$2 \text{ cm}^2 / \text{V s}\$ for electrons and \$0.1 \text{ cm}^2 / \text{V s}\$ for holes](#)


Appl. Phys. Lett. **94**, 162105 (2009); 10.1063/1.3119636

The advertisement features a background image of a person in a lab coat working with a complex piece of scientific equipment. Overlaid on the image are several text elements: 'WHAT YOU NEED TO KNOW ABOUT VACUUM' in yellow and white, 'WEBINAR SERIES' in white on a purple rectangular background, and 'SIGN UP TODAY' in white on a blue rectangular background. At the bottom, the Agilent Technologies logo and name are displayed on a blue background.

WHAT YOU NEED
TO KNOW ABOUT VACUUM

WEBINAR SERIES

SIGN UP TODAY

 **Agilent Technologies**

Breaking network connectivity leads to ultralow thermal conductivities in fully dense amorphous solids

Jeffrey L. Braun,¹ Sean W. King,² Ashutosh Giri,¹ John T. Gaskins,¹ Masanori Sato,³ Takemasa Fujiseki,³ Hiroyuki Fujiwara,³ and Patrick E. Hopkins^{1,a)}

¹Department of Mechanical and Aerospace Engineering, University of Virginia, Charlottesville, Virginia 22904, USA

²Intel Corporation, Logic Technology Development, 5200 NE Elam Young Parkway, Hillsboro, Oregon 97124, USA

³Department of Electrical, Electronic and Computer Engineering, Gifu University, 1-1 Yanagido, Gifu 501-1193, Japan

(Received 16 September 2016; accepted 19 October 2016; published online 8 November 2016)

We demonstrate a method to reduce the thermal conductivity of fully dense (above the rigidity percolation threshold) amorphous thin films below the minimum limit by systematically changing the coordination number through hydrogenation. Studying a-SiO:H, a-SiC:H, and a-Si:H thin films, we measure the thermal properties using time-domain thermoreflectance to show that thermal conductivity can be reduced below the amorphous limit by a factor of up to two. By experimentally investigating the thermophysical parameters that determine thermal conductivity, we show that sound speed, atomic density, and heat capacity cannot explain the measured reduction in thermal conductivity, revealing that the coordination number can significantly alter the scattering length scale of heat carriers. Reformulating the minimum limit to consider the propensity for energy to transfer through the non-hydrogen network of atoms, we observe greatly improved agreement with experimental data. *Published by AIP Publishing.* [<http://dx.doi.org/10.1063/1.4967309>]

In the search for ultralow thermal conductivity materials, many approaches have been taken to obtain thermal conductivities below the theoretical minimum limit of fully dense solids used to describe thermal transport in the amorphous materials and glasses.¹ In this “amorphous limit” of vibrational thermal conductivity, energy transport is limited to a random walk of atomic vibrations,² effectively limiting the length scale of energy exchange to the order of the average atomic spacing. Various approaches have demonstrated the ability to surpass this amorphous limit in crystalline or quasi-crystalline fully dense solids through introducing nanostructured material interfaces^{3–9} and/or reducing the interatomic bonding environment,^{5,10–13} which effectively creates a crystal of Einstein oscillators.^{2,13}

The principle of reducing a crystalline material’s thermal conductivity below the amorphous limit relies on the reduction of phonon scattering times by exploiting the spectral nature of phonons via the aforementioned manipulation of interfaces and bonding environments across various length scales. Reducing the thermal conductivity of fully dense solids already in the amorphous phase, however, has been proven to be much more difficult. The already spatially limited distances of vibrational energy exchange define the length scales over which the amorphous solid must be manipulated in order to create further reductions in thermal conductivity beyond its amorphous limit. Typically, reductions in the thermal conductivity of amorphous solids have been realized via changes in the atomic density or introduction of porosity.^{14–18} This approach relies on simple scaling of the amorphous solid’s thermal conductivity with density, as well established via differential effective medium theory.

Reducing the thermal conductivity of an amorphous solid without significant reductions in atomic density therefore must take a different approach.

Thermal transport in amorphous semiconductors is described by vibrational modes of propagating, delocalized “propagons,” non-propagating, delocalized “diffusons,” and non-propagating, localized “locons.”^{19–22} In the case of thin films, we previously showed that diffusons are the primary contributors to cross-plane thermal transport in amorphous silicon (a-Si) due to the suppression of propagons from interfacial scattering,²³ revealing that for a-Si without doping, the minimum thermal conductivity model sufficiently describes the diffuson contribution to thermal conductivity. However, the addition of mass defects, changes in bond structure via additional elements, and disruptions in network connectivity through changing coordination number collectively present a new approach to reduce thermal conductivity. To this end, in this study, we demonstrate that manipulating connectivity directly influences thermal conductivity in the 200 nm thin film hydrogenated amorphous silicon (a-Si:H), silicon oxide (a-SiO:H), and silicon carbide (a-SiC:H) samples (collectively denoted as a-Si[O/C]:H) deposited on crystalline silicon (c-Si) substrates. Moreover, we show that reducing the coordination number allows for a reduction beyond the minimum limit to thermal conductivity by nearly a factor of two. We use these results to explore the energy exchange length scales of heat carriers as a function of coordination number to reveal that breaking network connectivity directly reduces thermal conductivity through reduction in both group velocity and scattering length scale of heat carriers. By re-deriving the minimum limit to thermal conductivity to directly solve for an effective scattering distance for heat carriers, we show that this energy exchange length scale falls below the average interatomic

^{a)}Electronic mail: phopkins@virginia.edu

spacing, suggesting a need to revise this model to account for network connectivity. Doing so yields better agreement with experimental data and highlights the idea that heat flows through the covalently bonded network of non-hydrogen atoms.

Samples were fabricated using plasma-enhanced chemical vapor deposition (PECVD). Extensive characterization of mechanical and structural properties can be found in Ref. 24. We measured the thermal conductivity of these amorphous thin films using time domain thermoreflectance (TDTR), and the details and analyses for which are described elsewhere.^{25–27} Our specific setup is described in Ref. 28. This technique requires a thin metal film to be deposited onto a-Si[O/C]:H to serve as a transducer of optical energy to thermal energy; in this case, we thermally evaporate an 80 nm layer of aluminum (Al) onto the a-Si[O/C]:H film. We measure the ratio of the in-phase to out-of-phase voltage of the probe reflectance as a function of pump-probe delay time using pump and probe $1/e^2$ spot sizes (diameters) of 30 and 20 μm , respectively, while the pump pulses are modulated with multiple frequencies ranging from $f=1$ to 12 MHz in sinusoidally varying envelopes. Using a multilayer, radially symmetric thermal model,^{25,27} we fit for the thermal boundary conductance between the Al transducer and the amorphous film ($h_{K,\text{Al/a-Si[O/C]:H}}$) and the a-Si[O/C]:H thermal conductivity ($\kappa_{\text{a-Si}}$). We assume bulk values for the heat capacity of the Al transducer and c-Si substrate.^{29,30} Because the dominant thermal resistance in the system is that of the a-Si[O/C]:H layer, sensitivity to the a-Si[O/C]:H layer thermal conductivity, heat capacity dominate the signal that we measure during TDTR. We use multiple modulation frequencies to fit both thermal conductivity and heat capacity simultaneously³¹ to find that heat capacity remains relatively constant among samples (supplementary material), varying from 1.5 to 1.6 $\text{J cm}^{-3} \text{K}^{-1}$.

Thermal conductivity, κ , values are shown in Fig. 1 as a function of several film properties, namely, (a) silicon content, (b) hydrogen content, (c) elastic modulus, as determined by nano-indentation, and (d) coordination number, $\langle r \rangle$, as determined by combined nuclear reaction analysis (NRA) with the Rutherford backscattering (RBS),³² to reveal interesting insight into the origin of the difference in thermal conductivities among samples. First, it is clear that increasing silicon

content directly correlates with increasing thermal conductivity, while increasing hydrogen content has the opposite effect. More interesting, though, is the fact that the increasing silicon content dominates both the a-SiO:H and a-SiC:H samples in determining thermal conductivity. In the case of hydrogenation, however, it is clear that addition of hydrogen affects a-SiO:H and a-SiC:H differently, causing a stronger reduction in the case of a-SiO:H with the same hydrogen content. Second, elastic modulus and thermal conductivity are directly related, a reasonable observation considering that elastic modulus is related to the average bond strength among atoms. However, as we will discuss below, this bond strength, considered when using group velocity to model thermal conductivity, does not explain the vast difference in thermal conductivities among samples. Finally, increasing coordination number correlates with increasing thermal conductivity. This is consistent with the previous studies^{33,34} that apply the rigidity percolation theory of Phillips and Thorpe^{35,36} to understand this relation. Ghossoub *et al.*³³ reasoned that $\kappa \propto v_L \propto E^{1/2} \propto \langle r \rangle^{3/4}$ (where v_L is longitudinal sound speed) to show agreement with the experimental data. This reasoning assumes that $\langle r \rangle$ only affects v_L , which works well for network chains like amorphous fluorocarbons (the carbon-fluorine bond breaks the network in the same way that silicon-hydrogen bonds do in a-Si:H). However, in this work, we introduce oxygen, carbon, and hydrogen contents to entirely change the network, as silicon-oxygen and silicon-carbon are non-terminating, meaning network connectivity is broken through hydrogen termination and silicon-silicon networks are further disrupted through oxygen and carbon inclusion.

Despite the insight into the mechanisms driving the measured thermal conductivities, further analysis is needed to understand the effect of structure on thermal transport in these amorphous networks. To this end, we apply a kinetic theory model, which we extend to the minimum thermal conductivity model.¹ We re-derive this model below to understand the inherent assumptions on the nature of bonding and scattering length scales of heat carrying vibrational modes, beginning with the simple kinetic theory relation describing thermal conductivity

$$\kappa = \sum_j \frac{1}{3} C_j v_j \lambda_j, \quad (1)$$

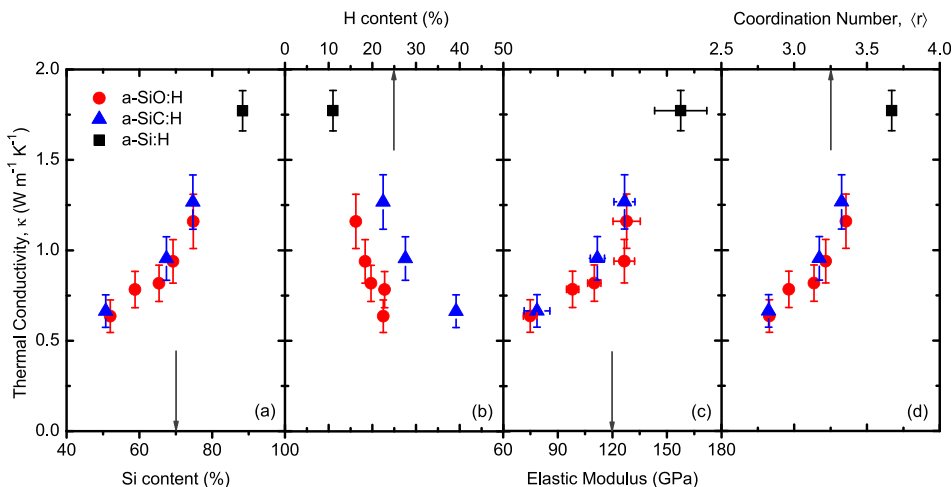


FIG. 1. Thermal conductivity, κ , as a function of (a) silicon content, (b) hydrogen content, (c) elastic modulus, and (d) coordination number, $\langle r \rangle$. Filled circles represent a-SiO:H, filled triangles represent a-SiC:H, and filled squares represent a-Si:H. Arrows point to the x-axis associated with each set of thermal conductivity data.

where j is the polarization (one longitudinal, two transverse), C is the volumetric heat capacity, v is the group velocity (assumed to be sound speed), and λ is the scattering mean free path of heat carriers in the system. This simple relation is powerful in its revelation of the key components that govern thermal conductivity – it is proportional to heat capacity, sound speed, and mean free path, meaning the observed differences in thermal conductivity among samples are due to differences in one or more of these parameters among samples. We note that heat capacity among samples is relatively constant, changing by less than 10% among samples, as measured via TDTR ([supplementary material](#)). This difference will be captured below when considering the number densities and sound speeds. We proceed with expanding this expression, noting that volumetric heat capacity can be described by

$$C_j = \int_0^{\omega_{D,j}} \hbar \omega D_j(\omega) \frac{\partial f_{BE}}{\partial T} d\omega$$

$$= \frac{\hbar^2}{2\pi^2 k_B T^2 v_j^3} \int_0^{\omega_{D,j}} \omega^4 \frac{\exp\left(\frac{\hbar\omega}{k_B T}\right)}{\left(\exp\left(\frac{\hbar\omega}{k_B T}\right) - 1\right)^2} d\omega, \quad (2)$$

where ω_D is the Debye frequency (the maximum frequency of vibration of polarization j), \hbar is the reduced Planck's constant, $D_j = \omega^2/2\pi^2 v_j^3$ is the density of states, f_{BE} is the Bose-Einstein distribution function, k_B is Boltzmann's constant, and T is temperature (293 K). Substituting Eq. (2) into Eq. (1), the thermal conductivity is

$$\kappa = \frac{\hbar^2}{6\pi^2 k_B T^2} \sum_j \frac{1}{v_j^2} \int_0^{\omega_{D,j}} \lambda_j \omega^4 \frac{\exp\left(\frac{\hbar\omega}{k_B T}\right)}{\left(\exp\left(\frac{\hbar\omega}{k_B T}\right) - 1\right)^2} d\omega. \quad (3)$$

The minimum thermal conductivity model is derived from this general model with two key assumptions. First, the Debye frequency is defined by $\omega_{D,j} = v_j(6\pi^2 n)^{\frac{1}{3}}$, where n is number density. With this model, the number density inherently defines the length scale of energy exchange. The second assumption is that $\lambda_j = \pi v_j/\omega$, or, in other words, the scattering time is half the period of oscillation for a given mode. The conventional model employs atomic number density such that atoms are indistinguishable and act as harmonic oscillators; we will return to this assumption later. Under these assumptions, the minimum thermal conductivity is defined as

$$\kappa_{\min} = \frac{\hbar^2}{6\pi^2 k_B T^2} \sum_j \frac{1}{v_j} \int_0^{v_j(6\pi^2 n)^{\frac{1}{3}}} \omega^3 \frac{\exp\left(\frac{\hbar\omega}{k_B T}\right)}{\left(\exp\left(\frac{\hbar\omega}{k_B T}\right) - 1\right)^2} d\omega. \quad (4)$$

This formulation, which depends on both sound speed and number density, is often used to accurately predict the thermal conductivity of amorphous materials.¹ In this case, number density is derived by using measured density together

with atomic compositions of silicon, oxygen, carbon, and hydrogen, as determined by combined NRA-RBS. We quantify sound speed with two independent techniques, picosecond acoustics and nano-indentation. In picosecond acoustics, we use the 10–100 ps delay time regime of our thermoreflectance signal to measure longitudinal sound speed in the a-Si[O/C]:H films,^{37–39} while nano-indentation relies on relating elastic modulus to the longitudinal sound speed; further details can be obtained in the [supplementary material](#). As depicted in Fig. 2, we find excellent agreement between both the techniques.

With sound speed and number density characterized, we apply Eq. (4) to determine whether number density or sound speed can explain the differences in thermal conductivities among samples. As depicted in Fig. 3(a), this model, when using either a constant (average) number density and only considering sound speed ($\kappa_{\min}(v)$) or both experimentally determined number density and sound speed ($\kappa_{\min}(v, n)$), fails to capture the thermal conductivity trend observed. Indeed, the model over-predicts the thermal conductivity for all but two samples.

Figure 1 revealed that many interconnected variables differ among samples; from a thermal transport perspective, bond strength, number density, and atomic composition can all play a role in determining thermal conductivity. The minimum thermal conductivity model given by Eq. (4) incorporates the parameters determined by these factors – bond strength effects are established through group velocity and number density is directly related to the Debye frequency. Atomic composition is not directly established in the model, as the model does not distinguish between the atom types in determining scattering times; note that mass-impurity scattering directly influences phonon scattering times in crystals. However, since scattering time in this model is already limited to half a period of oscillation, mass impurity scattering

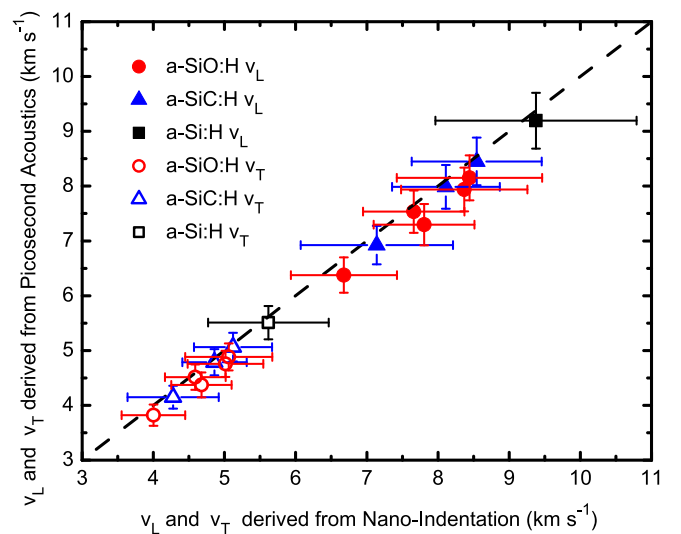


FIG. 2. Longitudinal (v_L) and transverse (v_T) sound speeds derived using picosecond acoustics (y-axis) vs. those derived using nano-indentation (x-axis). Equation (S1) is used to derive v_L from the nano-indentation results on elastic modulus, while sub-100 ps reflectance signals were used to measure v_L directly in the case of picosecond acoustics. To obtain v_T , Eq. (S2) is used to derive this quantity for both picosecond acoustics and nano-indentation. Details can be found in the [supplementary material](#).

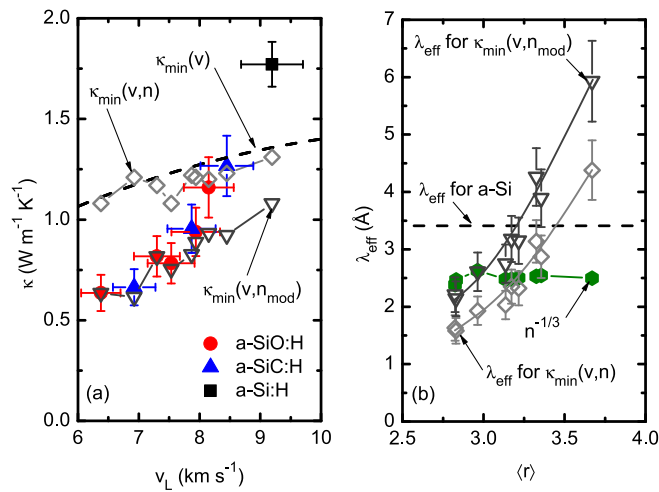


FIG. 3. (a) Thermal conductivity (κ) as a function of longitudinal sound speed (v_L): experimentally determined values of κ are plotted for the a-SiO:H (circles), a-SiC:H (triangles), and a-Si:H (square) samples. Plotted as a dashed line is the minimum thermal conductivity (κ_{\min}) model given by Eq. (4) with a constant number density equal to the mean value among samples. Hollow diamonds represent this same κ_{\min} model with the experimentally determined number density and sound speeds as inputs. Finally, hollow inverted triangles represent the same κ_{\min} , using a modified number density, $n_{\text{mod}} = n(1 - [\%H])$, which only accounts for non-hydrogen elements. (b) Effective scattering distance, λ_{eff} , determined using Eq. (3) vs. coordination number, $\langle r \rangle$. λ_{eff} is calculated for the minimum thermal conductivity model incorporating number density directly ($\kappa_{\min}(v, n)$) and modified number density ($\kappa_{\min}(v, n_{\text{mod}})$); solid lines serve to guide the eye. Shown also is λ_{eff} for a-Si (dashed line) and the average interatomic spacing (solid hexagons) as determined by $n^{-1/3}$.

is not expected to influence thermal transport. This can be further justified by comparing predicted and experimental values of multi-component systems such as SiO₂, CdGeAs₂, and As₂S₃.¹ Given the well characterized parameters that go into the model, disagreement with the experimental thermal conductivities suggests that the scattering length scale of heat carriers is being reduced below that assumed by the conventional minimum limit. Referring back to Eq. (3), we now solve for this scattering length scale, denoted by $\lambda_j = \lambda_{\text{eff}}$ for effective scattering distance, to understand how this changes among samples. This is the same concept as defining a “gray” mean free path for describing the phonons in crystals. We emphasize that this length scale is “effective” because it is derived from the same convention that defines the minimum limit and so inherits all the assumptions and limitations that come with it.

As depicted in Fig. 3(b), the effective scattering distances range from ~ 1.5 to 4.5 Å when the conventional model ($\kappa_{\min}(v, n)$) is employed. To understand the significance of this length scale, the average interatomic spacing, as determined by $n^{-1/3}$, is shown to reveal that this effective scattering distance is reduced below the average interatomic spacing. For reference, the average interatomic spacing of a-Si is ~ 2.7 Å, while the effective mean free path for a-Si having a thermal conductivity of $1.0 \text{ W m}^{-1} \text{ K}^{-1}$ is ~ 3.4 Å. The idea of the effective scattering length scale falling below the average interatomic spacing is not physically sound, implying that the model used does not appropriately describe our data. Thus, we turn back to Eq. (4) to answer the following fundamental question: do all atoms behave as harmonic

oscillators? We argue that if heat moves through the network of covalently bonded silicon, oxygen, and carbon, then hydrogen does not contribute to thermal transport. Stated differently, energy traverses the covalently bonded network but necessarily scatters at hydrogen termination sites. This is a similar argument for using the molecular number density vs. atomic density to describe the minimum limit in the layered crystalline systems of molecular building blocks.^{40–43} These models assume that molecules vibrate such that intermolecular vibrations do not transport heat; in this way, molecules, rather than atoms, act as harmonic oscillators in the minimum limit derivation. In this case, hydrogen can be thought to vibrate with its bonded neighbor as a single molecular oscillator such that intermolecular vibrations do not contribute to heat conduction. Under this hypothesis, we calculate κ_{\min} by assuming a modified number density defined by $n_{\text{mod}} = n(1 - [\%H])$. The results, presented as $\kappa_{\min}(v, n_{\text{mod}})$ in Fig. 3(a), show an excellent agreement with the data for all but the highest three thermal conductivities, suggesting this model more appropriately describes the minimum limit to thermal conductivity. Moreover, the effective scattering length scale, as shown in Fig. 3(a), now, within uncertainty, approaches the interatomic spacing only in the limit of the lowest thermal conductivity samples.

The primary conclusions of this study are as follows: (1) the energy exchange length scales of heat carriers in amorphous solids can vary based on local structure, (2) this length scale can be directly manipulated such that thermal conductivity can be reduced below the conventional minimum limit, and (3) this conventional minimum limit implies such length scales fall below the average interatomic spacing, but when altered under the hypothesis that heat is carried only by the non-hydrogen network of atoms, the minimum limit more accurately captures experimental data. Previous computational works^{19,44,45} have shown that heat carriers in amorphous systems can have a range of scattering times and distances. Just as nanostructures and boundaries can be used in crystalline systems to reduce the scattering lengths of phonons through incoherent scattering, the spectral nature of heat carriers in amorphous solids can be similarly exploited to reduce their scattering lengths; the key to such reduction is the manipulation of structure on the order of intrinsic scattering length scales. In this study, we have demonstrated that breaking network connectivity provides a means for reducing the effective scattering length scale of these heat carriers, leading to thermal conductivities below the conventional amorphous limit.

See [supplementary material](#) for additional experimental details, including characterization of sound speed and volumetric heat capacity.

We appreciate the support from the Office of Naval Research, Grant No. N00014-15-12769.

¹D. G. Cahill, S. K. Watson, and R. O. Pohl, *Phys. Rev. B* **46**, 6131 (1992).
²A. Einstein, *Ann. Phys.* **340**, 898 (1911).
³R. M. Costescu, D. G. Cahill, F. H. Fabreguette, Z. A. Sechrist, and S. M. George, *Science* **303**, 989 (2004).
⁴G. Pernot, M. Stoffel, I. Savic, F. Pezzoli, P. Chen, G. Savelli, A. Jacquot, J. Schumann, U. Denker, I. Mönch, C. Deneke, O. G. Schmidt, J. M.

- Rampnoux, S. Wang, M. Plissonnier, A. Rastelli, S. Dilhaire, and N. Mingo, *Nat. Mater.* **9**, 491 (2010).
- ⁵C. Chiritescu, D. G. Cahill, N. Nguyen, D. Johnson, A. Bodapati, P. Keblinski, and P. Zschack, *Science* **315**, 351 (2007).
- ⁶M. D. Losego, I. P. Blitz, R. A. Vaia, D. G. Cahill, and P. V. Braun, *Nano Lett.* **13**, 2215 (2013).
- ⁷P. E. Hopkins, M. Mittal, L. M. Phinney, A. M. Grillet, and E. M. Furst, *Appl. Phys. Lett.* **99**, 133106 (2011).
- ⁸A. Giri, J.-P. Niemelä, T. Tynell, J. T. Gaskins, B. F. Donovan, M. Karppinen, and P. E. Hopkins, *Phys. Rev. B* **93**, 115310 (2016).
- ⁹Y. S. Ju, M.-T. Hung, M. J. Carey, M.-C. Cyrille, and J. R. Childress, *Appl. Phys. Lett.* **86**, 203113 (2005).
- ¹⁰J. C. Duda, P. E. Hopkins, Y. Shen, and M. C. Gupta, *Appl. Phys. Lett.* **102**, 251912 (2013).
- ¹¹J. C. Duda, P. E. Hopkins, Y. Shen, and M. C. Gupta, *Phys. Rev. Lett.* **110**, 015902 (2013).
- ¹²X. Wang, C. D. Liman, N. D. Treat, M. L. Chabynec, and D. G. Cahill, *Phys. Rev. B* **88**, 075310 (2013).
- ¹³J. R. Olson, K. A. Topp, and R. O. Pohl, *Science* **259**, 1145 (1993).
- ¹⁴C. S. Gorham, J. T. Gaskins, G. N. Parsons, M. D. Losego, and P. E. Hopkins, *Appl. Phys. Lett.* **104**, 253107 (2014).
- ¹⁵P. E. Hopkins, B. Kaehr, L. M. Phinney, T. P. Koehler, A. M. Grillet, D. Dunphy, F. Garcia, and C. J. Brinker, *J. Heat Transfer* **133**, 061601 (2011).
- ¹⁶P. E. Hopkins, B. Kaehr, E. S. Piekos, D. Dunphy, and C. J. Brinker, *J. Appl. Phys.* **111**, 113532 (2012).
- ¹⁷A. J. Bullen, K. E. O'Hara, D. G. Cahill, O. Monteiro, and A. von Keudell, *J. Appl. Phys.* **88**, 6317 (2000).
- ¹⁸R. M. Costescu, A. J. Bullen, G. Matamis, K. E. O'Hara, and D. G. Cahill, *Phys. Rev. B* **65**, 094205 (2002).
- ¹⁹J. M. Larkin and A. J. H. McGaughey, *Phys. Rev. B* **89**, 144303 (2014).
- ²⁰P. B. Allen, J. L. Feldman, J. Fabian, and F. Wooten, *Philos. Mag.* **B 79**, 1715 (1999).
- ²¹J. L. Feldman, P. B. Allen, and S. R. Bickham, *Phys. Rev. B* **59**, 3551 (1999).
- ²²P. B. Allen and J. L. Feldman, *Phys. Rev. B* **48**, 12581 (1993).
- ²³J. L. Braun, C. H. Baker, A. Giri, M. Elahi, K. Artyushkova, T. E. Beechem, P. M. Norris, Z. C. Leseman, J. T. Gaskins, and P. E. Hopkins, *Phys. Rev. B* **93**, 140201 (2016).
- ²⁴M. Sato, S. W. King, W. A. Lanford, P. Henry, T. Fujiseki, and H. Fujiwara, *J. Non-Cryst. Solids* **440**, 49 (2016).
- ²⁵D. G. Cahill, *Rev. Sci. Instrum.* **75**, 5119 (2004).
- ²⁶A. J. Schmidt, *Annu. Rev. Heat Transfer* **16**, 159 (2013).
- ²⁷P. E. Hopkins, J. R. Serrano, L. M. Phinney, S. P. Kearney, T. W. Grasser, and C. T. Harris, *J. Heat Transfer* **132**, 081302 (2010).
- ²⁸R. Cheaito, C. S. Gorham, A. Misra, K. Hattar, and P. E. Hopkins, *J. Mater. Res.* **30**, 1403 (2015).
- ²⁹Y. S. Touloukian, R. W. Powell, C. Y. Ho, and P. G. Klemens, *Thermophysical Properties of Matter—Specific Heat: Non-Metallic Solids* (IFI/Plenum, New York, 1970), Vol. 5.
- ³⁰Y. S. Touloukian and E. H. Buyco, *Thermophysical Properties of Matter—Specific Heat: Metallic Elements and Alloys* (IFI/Plenum, New York, 1970), Vol. 4.
- ³¹J. Liu, J. Zhu, M. Tian, X. Gu, A. Schmidt, and R. Yang, *Rev. Sci. Instrum.* **84**, 034902 (2013).
- ³²W. A. Lanford, M. Parenti, B. J. Nordell, M. M. Paquette, A. N. Caruso, M. Mäntymäki, J. Hämäläinen, M. Ritala, K. B. Klepper, V. Miiikkulainen, O. Nilsen, W. Tenhaeff, N. Dudney, D. Koh, S. K. Banerjee, E. Mays, J. Bielefeld, and S. W. King, in *The 22nd International Conference on Ion Beam Analysis, IBA, 2015* [Nucl. Instrum. Methods Phys. Res., Sect. B **371**, 211 (2016)].
- ³³M. G. Ghossoub, J.-H. Lee, O. T. Baris, D. G. Cahill, and S. Sinha, *Phys. Rev. B* **82**, 195441 (2010).
- ³⁴S. W. King, J. Bielefeld, G. Xu, W. A. Lanford, Y. Matsuda, R. H. Dauskardt, N. Kim, D. Hondongwa, L. Olasov, and B. Daly, *J. Non-Cryst. Solids* **379**, 67 (2013).
- ³⁵J. C. Phillips, *J. Non-Cryst. Solids* **34**, 153 (1979).
- ³⁶M. Thorpe, *J. Non-Cryst. Solids* **57**, 355 (1983).
- ³⁷C. Thomsen, H. T. Grahn, H. J. Maris, and J. Tauc, *Phys. Rev. B* **34**, 4129 (1986).
- ³⁸G. A. Antonelli, B. Perrin, B. C. Daly, and D. G. Cahill, *MRS Bull.* **31**, 607 (2006).
- ³⁹D. Hondongwa, L. Olasov, B. Daly, S. King, and J. Bielefeld, *Thin Solid Films* **519**, 7895 (2011).
- ⁴⁰P. E. Hopkins and E. S. Piekos, *Appl. Phys. Lett.* **94**, 181901 (2009).
- ⁴¹M. A. Panzer, M. Shandalov, J. A. Rowlette, Y. Oshima, Y. W. Chen, P. C. McIntyre, and K. E. Goodson, *IEEE Electron Device Lett.* **30**, 1269 (2009).
- ⁴²P. E. Hopkins and T. E. Beechem, *Nanoscale Microscale Thermophys. Eng.* **14**, 51 (2010).
- ⁴³B. M. Foley, H. J. Brown-Shaklee, M. J. Campion, D. L. Medlin, P. G. Clem, J. F. Ihlefeld, and P. E. Hopkins, *J. Am. Ceram. Soc.* **98**, 624 (2015).
- ⁴⁴W. Lv and A. Henry, *Appl. Phys. Lett.* **108**, 181905 (2016).
- ⁴⁵W. Lv and A. Henry, *New J. Phys.* **18**, 013028 (2016).